Grasp Synergies: Data Gathering and Analysis

Marco Gabiccini* and Georg Stillfried*, Hamal Marino, Matteo Bianchi

***Abstract*—This paper presents a methodology to accurately record human finger postures during grasping. The main contribution consists of a kinematic model of the human hand reconstructed via magnetic resonance imaging of one subject that (i) is fully parameterized and can be adapted to different subjects, and (ii) is amenable of in-vivo to joint angle recordings via optical tracking of markers attached to the skin. The principal novelty here is the introduction of a soft-tissue artifact compensation mechanism that can be optimally calibrated in a systematic way. The high-quality data gathered are employed to study the properties of hand *postural synergies* in humans, for the sake of ongoing neuro-science investigations. These data are analyzed and some comparison with similar studies are reported. After a meaningful mapping strategy has been devised, these data could be employed to define robotic hand postures amenable to attain effective grasps, or could be used as prior knowledge in lower-dimensional, real-time avatar hand animation.**

I. Introduction

In the field of robotic grasping with anthropomorphic hands, robots can learn from the way human grasp. For example, *postural synergies* [1] utilized by the human can be mapped to a robotic hand, so that hand postures can be more easily commanded. This paper deals with the challenge of how to suitably record human finger postures during grasps. On the one hand, it is desirable to have a low-dimensional representation of the posture. This can be achieved for example by using a data glove. On the other hand, the poses of the finger segments should be measured with high accuracy. For this, optical position measurements of skin markers can be used. To combine high accuracy with low data dimensionality, optical position measurements need to be combined with an accurate kinematic model of the hand. Commonly, such models are constructed of serial chains of rotation axes whose positions and orientations are modified by rotations around these axes, but which are otherwise fixed. This kind of kinematics is quite suitable for modelling the movement of the skeleton. However, the skin moves relative to the bones, introducing a soft tissue artifact (STA) when measuring skeletal movement by tracking skin markers.

In our previous work [2], magnetic resonance imaging (MRI) was used to measure the actual amount of STA in different hand postures and on different parts of the dorsal skin of the hand and fingers. It turned out that STA is particularly large near joints.

Zhang et al. [3] proposed a model of the skin motion that occurs near joints. Essentially, the model states that the movement of the skin is smaller, but proportional to the movement of the adajcent bone. The model by Zhang et al. is two-dimensional, considering only movement in the flexion/extension plane. Here, the model is extended to three spatial dimensions, considering the skin movement near joints with one as well as two degrees of freedom (DoF). The skin movement model is validated using aforementioned MRI data as ground truth.

The skin movement model is incorporated into a 26-DoF kinematic hand model, where the geometric transformations from one bone/joint frame to another, as well as to the associated markers, are implemented using a twist or matrix exponential parametrization, which has become standard in robotic applications [4], [5].

This model allows to take into account the differences between hands of different subjects, by suitably estimating hand geometrical and dimensional parameters with a calibration phase that minimizes the residual between measured and estimated bone poses.

An algorithm is developed to reconstruct the joint angles of large movements, given the estimated geometical and dimensional parameters. For this, an Extended Kalman Filter using a Gauss-Newton minimization procedure with Levenberg-Marquardt adjustment for the step length is used. The algorithm takes advantage of the fact that the Jacobian matrix can be computed particularly straightforward using matrix exponential parametrization.

The proposed methods are used to reconstruct hand postures during grasps of imagined objects. The reconstructed poses are then analyzed by means of Principal Component Analysis in order to study postural synergies, i.e. covariation schemes in inter-digit joint positions [1]. Results are compared with the ones described in [6], where authors focused on central contributions to hand posture modulation, analyzing a large number of different imagined grasped objects.

II. Description of the kinematic model

The kinematic model of the human hand with respect to the forearm is devised as a *kinematic tree*, whose root node consists of the Cartesian reference frame $\{B\}$ (rigidly attached to a bracelet fastened to the forearm) and whose leaves are the frames fixed to the distal phalanxes of the five fingers, as depicted in Figure 1. The five paths to the leaf nodes (phalanxes distalis, PDs) of the tree have a common segment through the wrist joint, centered at point W, and then branch out from the MC_2 (metacarpal bone of the index) as serial kinematic chains.

This work is supported by the European Commission under CP grant no. 248587, "THE Hand Embodied", within the FP7-ICT-2009-4-2-1 program "Cognitive Systems and Robotics" and by ERC Advanced Grant no. 291166 "SoftHands: A Theory of Soft Synergies for a New Generation of Artificial Hands".

M. Gabiccini is with the DICI and Res. Center "E. Piaggio" University of Pisa, 56122 Pisa, Italy, and with the Dep. of Advanced Robotics, Istituto Italiano di Tecnologia, via Morego, 30, 16163 Genova (phone: +39-050-221.80.77, fax: +39-050-221.80.65, email: m.gabiccini@ing.unipi.it)

G. Stillfried is with the Institute of Robotics and Mechatronics, German Aerospace Center (DLR), Münchner Straße 10, 82234 Weßling, Germany (Georg.Stillfried@dlr.de)

H. Marino and Matteo Bianchi are with the Res. Center "E. Piaggio", University of Pisa, 56122 Pisa, Italy, and with the Dep. of Advanced Robotics, Istituto Italiano di Tecnologia, via Morego, 30, 16163 Genova ({hamal.marino,matteo.bianchi}@centropiaggio.unipi.it)

*) Both starred authors contributed equally to the paper.

As an example, the relative motion of $\{\text{PD}_1\}$ with respect to $\{B\}$ is influenced by the rotation of joints ξ_{w_1}, ξ_{w_2} (two-DoF wrist joint), $\xi_{\text{CMC}_{1a}}$, $\xi_{\text{CMC}_{1b}}$ (two-DoF carpometacarpal ajoint), $\xi_{\text{MCP}_{1a}}$, $\xi_{\text{MCP}_{1b}}$ (two-DoF metacarpophalangeal joint), ξ_{IP_1} (one-DoF interphalangeal joint).

A. Hand posture parameterization

To efficiently parameterize the posture of the $j-$th phalanx in the $i-$th finger chain (here expressed as the pose of frame $\{F_{ij}\}$), we employ the *Product of Exponentials* (POE) formula [7], i.e.

$$g_{BF_{ij}}(\theta_i) = \left[\prod_{k=1}^{j} e^{\widehat{\xi}_{ik}\theta_{ik}}\right] g_{BF_{ij}}(0). \tag{1}$$

Here, the $\widehat{\xi}_{ik}$'s are the twists of the joints defining the kinematic chain of the $i-$th finger, $\theta_i = [\theta_{i1} \cdots \theta_{ik} \cdots \theta_{ij}]^T$ are the exponential coordinates of the 2$^{\text{nd}}$ kind [4] for a local representation of SE(3) for the $j-$th phalanx in the $i-$th finger, and $g_{PB_{ij}}(0)$ is its initial configuration. We cast the set of local parameterizations (joint angles) needed for describing the postures of all the fingers in the vector $\theta = [\theta_1^T \cdots \theta_5^T]^T$. It is worth noting that $i = 1, \ldots, 5$, since the human hand has five fingers, while $j \in \mathcal{I}(j)$, where $\mathcal{I}(j)$ is the set of the indices (in the form of labels) of the parent joints to the $j-$th phalanx in its kinematic chain. As an example, if we consider $j = \text{PP}_1$, the set of indices becomes $\mathcal{I}(j) = \{w_1, w_2, \text{CMC}_{1a}, \text{CMC}_{1b}, \text{MCP}_{1a}, \text{MCP}_{1b}\}$.

In accordance with the definition of Eq. (1), it is worth noting that the twist components have to be expressed in the common base frame $\{B\}$ and in the reference posture for the hand, i.e. when $\theta_{ik} = 0$. Therefore, it is possible to write more explicitly $\xi_{ij} = {}^b\xi_{ij}$, where the left superscript describes the *reading* frame, in accordance with [8]. Should the joint twist be more easily expressed in an auxiliary (possibly moving) frame $\{A(\theta)\}$, we could profitably recover its components in $\{B\}$, in the reference configuration, by employing the formula

$${}^b\xi_{ij} = \text{Ad}_{g_{ba}(0)}\, {}^a\xi_{ij}, \tag{2}$$

where $g_{ba}(0)$ is the posture of $\{A(0)\}$ w.r.t. $\{B\}$ in the reference configuration and the *Adjoint* transformation $\text{Ad}_g : \mathbb{R}^6 \to \mathbb{R}^6$ is a map between different expressions of the *same* twist in different *reading* reference frames.

B. Hand velocity parameterization

The POE parameterization of the hand posture can be profitably employed for computing the *rigid-body* velocity of each phalanx. As we shall see, this quantity is key for systematically calculating the linear velocity of the optical markers attached to the bone or to the skin.

The rigid-body velocity $\widehat{V}^{F_{ij}}_{BF_{ij}}$ of $\{F_{ij}\}$ in the moving frame $\{F_{ij}\}$ is given (as a 4×4 matrix) by the following formula

$$\widehat{V}^{F_{ij}}_{BF_{ij}} := g^{-1}_{BF_{ij}} \dot{g}_{BF_{ij}} = \begin{bmatrix} \widehat{\omega}^{F_{ij}}_{BF_{ij}} & v^{F_{ij}}_{BF_{ij}} \\ 0 & 0 \end{bmatrix} \tag{3}$$

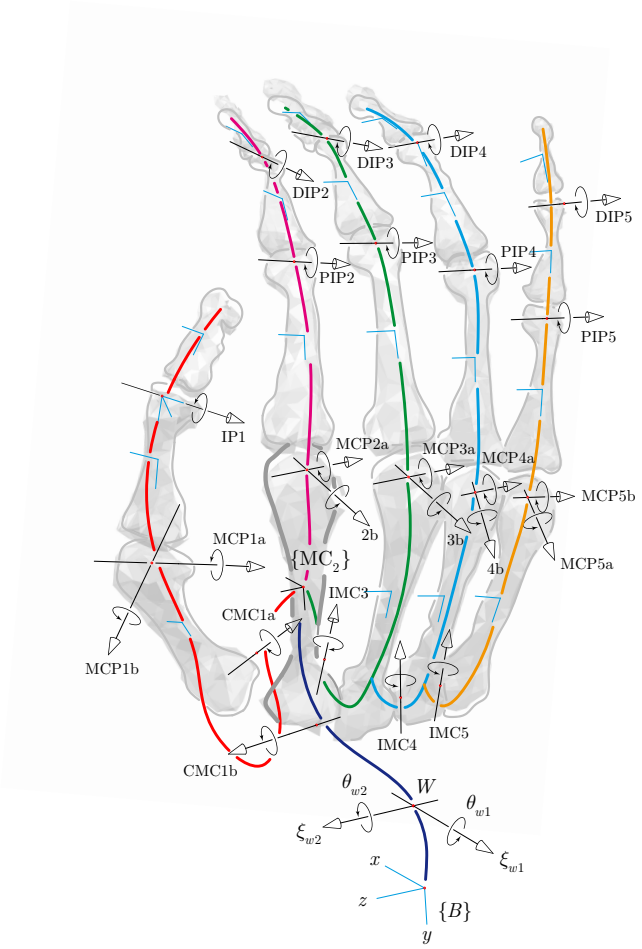

Fig. 1: Human hand kinematic model.

where $\widehat{\omega}^{F_{ij}}_{BF_{ij}} := R^T_{BF_{ij}} \dot{R}_{BF_{ij}}$ is the skew-symmetric matrix of the angular velocity components (in $\{F_{ij}\}$) of $\{F_{ij}\}$ w.r.t. $\{B\}$, and $v^{F_{ij}}_{BF_{ij}} = R^T_{BF_{ij}} \dot{d}_{BF_{ij}}$ are the components (in $\{F_{ij}\}$) of the velocity of the origin $O_{F_{ij}}$ with respect to O_B. Equation (3) can be rewritten (as a 6×1 vector) in a convenient form by factoring out the joint velocities $\dot{\theta}_i$ of the $i-$th finger as follows

$$V^{F_{ij}}_{BF_{ij}} = J^{F_{ij}}_{BF_{ij}}(\theta_i)\, \dot{\theta}_i, \tag{4}$$

where the *distal Jacobian* $J^{F_{ij}}_{BF_{ij}}$ can be computed as $(k = 1, \ldots, j)$

$$J^{F_{ij}}_{BF_{ij}}(\theta_i) = [\xi_1^\dagger \cdots \xi_j^\dagger]; \quad \xi_k^\dagger = \text{Ad}^{-1}_{g_{k+1,F_{ij}}}\, \xi_k, \tag{5}$$

where we defined $g_{k+1,F_{ij}} := e^{\widehat{\xi}_{k+1}\theta_{k+1}} \cdots e^{\widehat{\xi}_j\theta_j} g_{BF_{ij}}(0)$, with $g_{j+1,F_{ij}} = g_{BF_{ij}}(0)$.

Since we will be interested in calculating the velocity $v^{B,[O_{F_{ij}}]}_{BF_{ij}}$ of the origin $O_{F_{ij}}$ w.r.t. O_B in $\{B\}$ components[1], we also

[1]It is worth observing that the apparently cumbersome expression $v^{B,[O_{F_{ij}}]}_{BF_{ij}}$ is simply $d/dt(p_{BF_{ij}})$. The indirect route followed for its derivation is due to the different meanings of the linear velocities $v^{F_{ij}}_{BF_{ij}}$ and $v^{B}_{BF_{ij}}$.

define the *hybrid* rigid-body velocity

$$V_{BF_{ij}}^{B,[O_{F_{ij}}]} := \begin{bmatrix} \widehat{\omega}_{BF_{ij}}^{B} & v_{BF_{ij}}^{B,[O_{F_{ij}}]} \\ 0 & 0 \end{bmatrix} = \mathrm{Ad}_{(R_{BF_{ij}},0)} V_{BF_{ij}}^{F_{ij}}. \quad (6)$$

A convenient form where the joint velocities $\dot{\theta}_i$ of the $i-$th finger are factored out is given by the following expression

$$V_{BF_{ij}}^{B,[O_{F_{ij}}]} = J_{BF_{ij}}^{B,[O_{F_{ij}}]}(\theta_i)\,\dot{\theta}_i, \quad (7)$$

where, defining $\xi_k^\sharp = \mathrm{Ad}_{(R_{BF_{ij}},0)}\,\mathrm{Ad}_{g_{F_{ij},k+1}}\,\xi_k$, the *hybrid Jacobian* $J_{BF_{ij}}^{B,[O_{F_{ij}}]}$ can be computed as $(k = 1, \ldots, j)$

$$J_{BF_{ij}}^{B,[O_{F_{ij}}]}(\theta_i) = [\xi_1^\sharp \cdots \xi_j^\sharp];, \quad (8)$$

C. Modelling bone markers

It is important to realize that frame $\{F_{ij}\}$ is a generic frame attached to the $j-$th phalanx of the $i-$th finger that is employed to express its global posture with respect to frame $\{B\}$. Should we prefer to use a different *local* frame, say $\{M_{ij}\}$, we could simply add a *local* transformation such that

$$g_{BM_{ij}}(\theta_i) = g_{BF_{ij}}(\theta_i) g_{F_{ij}M_{ij}} = \left[\prod_{k=1}^{j} e^{\widehat{\xi}_{ik}\theta_{ik}}\right] g_{BF_{ij}}(0) g_{F_{ij}M_{ij}}. \quad (9)$$

It is worth observing that frame $\{M_{ij}\}$ can be selected with origin coincident with the *optical marker* rigidly attached to the same phalanx, as shown in Figure 2 (a). In this case, only in the position of the origin of the frame $\{M_{ij}\}$ really matters. The components $p_{BM_{ij}}$ of the position vector $O_B O_{M_{ij}}$ in $\{B\}$ can be recovered by simply extracting it from the homogeneous transformation

$$g_{BM_{ij}}(\theta_i) = \begin{bmatrix} R_{BM_{ij}} & p_{BM_{ij}} \\ 0 & 1 \end{bmatrix} \quad (10)$$

It is worth observing that if $\{M_{ij}\}$ is selected to be parallel to $\{F_{ij}\}$, $g_{F_{ij}M_{ij}} = g_{F_{ij}M_{ij}}(a_b^{(ij)})$ where $a_B^{(ij)} \in \mathbb{R}^3$ is a translation vector defining the position of the marker attached to the bone w.r.t. the reference frame $\{F_{ij}\}$ attached to the bone. We cast all the parameters defining the position of all the *bone* markers with respect to each bone frame $\{F_{ij}\}$, $(i = 1, \ldots, 5;\ j \in \mathcal{I}(j))$ in vector a_B.

D. Modelling joint markers

For optical markers attached to areas of the back of the hand where the skin stretch with respect to the underlying bone is not negligible, a kinematic model considering the marker frame *fixed* with to some bone would be not motivated and would give poor results — errors due to this assumptions are generally referred to, in the literature, as *soft-tissue artifacts* (STA). The phenomenon of skin stretch is maximally evident in correspondence of joints, as shown by the experiments presented in Sec. [Georg's experiments]. In order to tackle this issue directly, we include in our model a skin stretch compensation mechanism that is biomechanically sound.

With reference to Figure 2 (b), we consider an optical marker attached to the skin above the MCP_1 joint. Let us denote such markers as *joint markers*. For brevity, we contemplate only the part of the kinematic chain from $\{\mathrm{MC}_2\}$ to $\{M\}$ and we set $1a = \mathrm{CMC}_{1a}$, $1b = \mathrm{CMC}_{1b}$, $2a = \mathrm{MCP}_{1a}$, $2b = \mathrm{MCP}_{1b}$. We consider the joint marker as being the leaf of a *virtual kinematic chain* described by the following equation

$$g_{l_0 m}(\theta) = e^{\widehat{\xi}_{1a}\theta_{1a}} e^{\widehat{\xi}_{1b}\theta_{1b}} e^{\widehat{\xi}_{2a}\tilde{\theta}_{2a}(\theta_{2a})} e^{\widehat{\xi}_{2b}\tilde{\theta}_{2b}(\theta_{2b})} g_{l0,2a} g_{2a,m}. \quad (11)$$

Equation (11) states that joint marker displacement is influenced by the rotations of the joints above which it is positioned, besides the rotations of the proximal joints. The main assumption made in (11) is that the twists describing the skin stretch mechanisms are *equal* to those defining the bone kinematics. However, the rotations of the last joint in the virtual chain $\tilde{\theta}_{2a}(\theta_{2a})$ and $\tilde{\theta}_{2b}(\theta_{2b})$ are (possibly nonlinear) functions of the joint angles θ_{2a} and θ_{2b}. This definition directly models the relative displacements of the skin with respect to the underlying bones. To keep things relatively simple we modeled the skin displacements by the following linear functions

$$\tilde{\theta}_{2a}(\theta_{2a}) = c_{2a}\theta_{2a}, \quad \tilde{\theta}_{2b}(\theta_{2b}) = c_{2b}\theta_{2b}. \quad (12)$$

Then, the constant *offset* transformation $g_{2a,m}$, accounting for the posture of the marker frame in the initial configuration, can be written as

$$g_{2a,m} = \begin{bmatrix} I & d_{2a,m} \\ 0^T & 1 \end{bmatrix}, \quad d_{2a,m} = [\rho\cos\delta \ \ \rho\sin\delta \ \ h]^T \quad (13)$$

and can be recovered by direct inspection of Figure (2). The other constant part $g_{l0,2a}$ is known from the kinematic chain in its initial configuration. It is worth observing that the displacement of each joint marker is characterized by the five parameters ρ, δ, h, c_{2a} and c_{2b}. The three parameters ρ, δ and h are the cylindrical coordinates of the marker position in the initial configuration, while c_{2a} and c_{2b} describe the skin displacement ($c_{2a} = c_{2b} = 0$, marker fixed to the proximal bone; $c_{2a} = c_{2b} = 1$, marker fixed to the distal bone). These kinds of parameters for all joint marker can be cast in the vector a_J and can be calibrated once as described in Sec. IV.

It is important to note that, given the joint marker direct kinematics described in eq. (11), the *rigid-body velocity* of the marker frame can be computed by combining the contributions of (i) the kinematic chain of the bones $J_{l0,m}^m$, and (ii) the Jacobian $\partial\tilde{\theta}/\partial\theta$ of the joint speeds $\tilde{\theta}$ of *virtual chain* with respect to the independent joint speeds θ as follows

$$V_{l0,m}^m(\theta, \dot{\theta}) = J_{l0,m}^m[\theta_{1a}, \theta_{1b}, \tilde{\theta}_{2a}(\theta_{2a}), \tilde{\theta}_{2b}(\theta_{2b})] \left.\frac{\partial\tilde{\theta}}{\partial\theta}\right|_{\tilde{\theta}(\theta)} \dot{\theta} \quad (14)$$

When the linear model in eq. (12) is adopted for the description the skin displacement, the explicit expression for $\partial\tilde{\theta}/\partial\theta$ is given by

$$\left.\frac{\partial\tilde{\theta}}{\partial\theta}\right|_{\tilde{\theta}(\theta)} = \mathrm{diag}(1, 1, c_{2a}, c_{2b}). \quad (15)$$

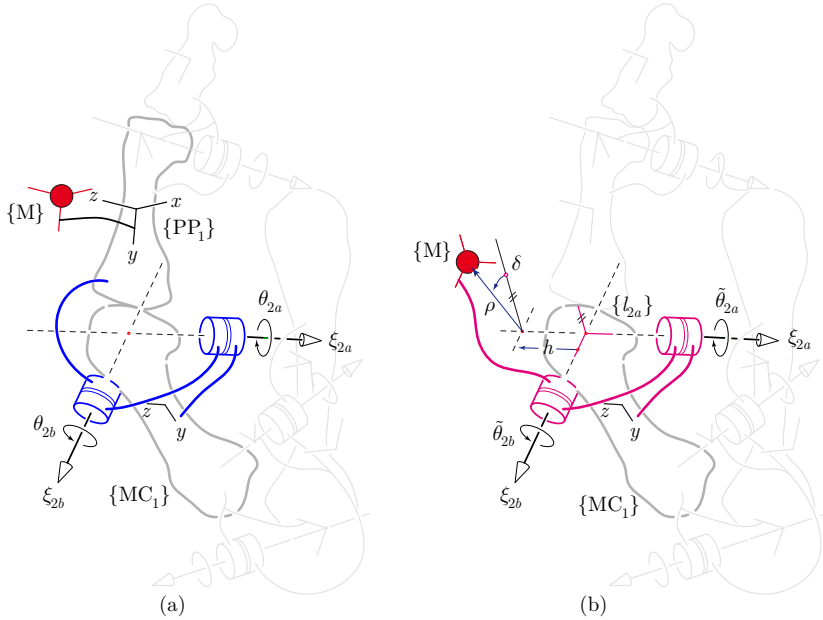

(a) (b)

Fig. 2: Models for: (a) markers attached to bones; (b) markers on a joint moving with the skin.

Then, the *hybrid* version of eq. (14), can be recovered as shown in eq. (7), and will be useful in the computation of the *residual Jacobian*, as it will be explained in Sec. V, eq. (24).

III. Validation of the Skin Movement Model Using Magnetic Resonance Imaging

We have used magnetic resonance imaging (MRI) to measure skin movement in dependence of bone movement [2]. Here we use the MRI data as ground truth to validate the skin movement model described in Sec. II-D.

A. Measurement of skin movement

MRI-sensitive Soledum oil capsules (Casella-med, Cologne, Germany; spheroids with diameter 7 mm and long axis 10 mm) are attached to the skin on the dorsal side of the hand of one subject (Fig. 3). For the validation of the skin movement model, the capsules centered over the metacarpophalangeal (MCP), proximal interphalangeal (PIP) and distal interphalangeal (DIP) joints are considered. MRI images of 20 different hand postures are recorded ($n_\mathrm{p} = 20$). The postures are chosen such that each joint is moved through its whole range of motion. The volumes of the bones and of the capsules are segmented from the MRI images.

One posture (flat hand) is designated as the reference posture. To give anatomical meaning to the marker movement, bone coordinate systems (BCS) are placed manually for each bone in the reference posture. According to the recommendations of the International Society of Biomechanics [9], the x-axis points in palmar direction, the y-axis in proximal and the z-axis in radial direction. The BCS of the bones in the other posture are determined using a point cloud registration algorithm by Hillenbrand [10].

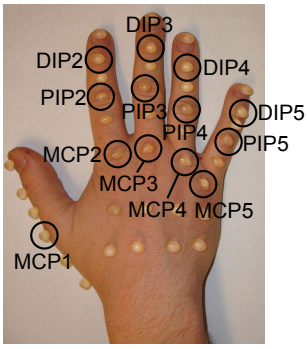

Fig. 3: Placement of the MRI-sensitive markers on the skin. For validating the marker movement model, markers near the MCP, PIP and DIP joints are considered.

The position of each skin marker is measured as the mean of the coordinates of the capsule volume weighted by the intensity values:

$$p_\mathrm{m} = \frac{1}{\sum_{i\in\mathcal{V}} g_i} \sum_{i\in\mathcal{V}} g_i x_i,$$

where $p_\mathrm{m} \in \mathbb{R}^3$ is the resulting vector containing the position coordinates of the skin marker, g_i is the intensity value (= grey value) at the i-th volume element of the capsule volume $\mathcal{V}$, and $x_i \in \mathbb{R}^3$ contains the coordinates of the i-th volume element.

The amount of uncompensated soft tissue artefact (STA) is quantified as the distance between the marker in the reference posture and the marker in another posture, both expressed in the BCS:

$$s_k = ||{}^\mathrm{P}p_{\mathrm{m},k} - {}^\mathrm{B}p_{\mathrm{m,ref}}||,$$

where s_k is the amount of uncompensated STA in posture k, ${}^\mathrm{B}p_{\mathrm{m},k}$ is the position of the marker with respect to bone B in posture k and ${}^\mathrm{B}p_{\mathrm{m,ref}}$ is the position of the marker with

respect to the bone in the reference posture. Note that the soft tissue artefact of markers on joints can be calculated with respect to either the proximal or the distal bone. Without loss of generality, we choose to calculate with respect to the proximal bone. The mean amount of uncompensated STA and its standard deviation over all postures is shown for each joint in the second column of Table I.

B. Identification of joint axes

Based on biomechanical literature, previous work [11] and everyday observation, the PIP and DIP joints are modelled with one axis of rotation (1 DoF), and the MCP joints with two intersecting orthogonal axes of rotation (2 DoF). The positions and orientations of the rotation axes are identified separately for each joint.

In 1-DoF joints, the modelled pose ${}^{\mathrm{P}}T_{\mathrm{D,mod},k}$ of the distal bone D with respect to the proximal bone P in posture k is results from a rotation of an initial pose ${}^{\mathrm{P}}T_{\mathrm{D},0}$ around the rotation axis of the joint:

$$ {}^{\mathrm{P}}T_{\mathrm{D,mod},k} = \mathrm{rot}_{4\times4}\left({}^{\mathrm{P}}p_{\mathrm{a1}},\, {}^{\mathrm{P}}a_1,\, q_{1k}\right)\, {}^{\mathrm{P}}T_{\mathrm{D},0}, $$

where ${}^{\mathrm{P}}p_{\mathrm{a1}} \in \mathbb{R}^3$ is a point on the rotation axis, ${}^{\mathrm{P}}a_1 \in \mathbb{R}^3$ is the Cartesian orientation of the rotation axis, q_1k is the joint angle in posture k and the operator $\mathrm{rot}_{4\times4}(p,a,q)$ produces a 4×4 rotation matrix that describes a general rotation around an axis defined by the orientation a, a point on the axis p and a rotation angle q:

$$ \mathrm{rot}_{4\times4}(p,a,q) = \begin{pmatrix} \mathrm{rot}_{3\times3}(a,q) & (p - \mathrm{rot}_{3\times3}(a,q)\,p) \\ 0\quad 0\quad 0 & 1 \end{pmatrix}, $$

where $\mathrm{rot}_{3\times3}(a,q)$ is a 3×3 matrix that describes a rotation around an axis with orientation a that passes through the origin of the coordinate system [12]:

$$ \mathrm{rot}_{3\times3}(a,q) = \begin{pmatrix} c + c'\,a_x^2, & c'\,a_x\,a_y - a_z\,s, & c'\,a_x\,a_z + a_y\,s \\ c'\,a_x\,a_y + a_z\,s, & c + c'\,a_y^2, & c'\,a_y\,a_z - a_x\,s \\ c'\,a_x\,a_z - a_y\,s, & c'\,a_y\,a_z + a_x\,s, & c + c'\,a_z^2 \end{pmatrix}, $$

with

$$ c = \cos q,\; c' = 1 - \cos q,\; s = \sin q, \\ a = (a_x, a_y, a_z)^{\mathrm{T}},\; \text{and}\; ||a|| = 1. $$

As initial pose, the measured pose in the reference posture is taken:

$$ {}^{\mathrm{P}}T_{\mathrm{D},0} = {}^{\mathrm{P}}T_{\mathrm{D,ref}}, $$

and the joint angles are defined to be zero in the reference posture.

In 2-DoF joints, the rotation takes place around two rotation axes:

$$ {}^{\mathrm{P}}T_{\mathrm{D,mod},k} = \mathrm{rot}_{4\times4}\left({}^{\mathrm{P}}p_{\mathrm{a1}},\, {}^{\mathrm{P}}a_1,\, q_{1k}\right) \\ \mathrm{rot}_{4\times4}\left({}^{\mathrm{P}}p_{\mathrm{a2}},\, {}^{\mathrm{P}}a_2,\, q_{2k}\right)\, {}^{\mathrm{P}}T_{\mathrm{D},0}. $$

The assumption of intersecting orthogonal axes imposes the following constraints:

$$ {}^{\mathrm{P}}p_{\mathrm{a1}} = {}^{\mathrm{P}}p_{\mathrm{a2}} \text{ and } {}^{\mathrm{P}}a_1\,{}^{\mathrm{P}}a_2 = 0. $$

The residual transformation $T_{\mathrm{diff},k}$ between the modelled bone pose ${}^{\mathrm{P}}T_{\mathrm{D,mod},k}$ and the measured bone pose ${}^{\mathrm{P}}T_{\mathrm{D},k}$ is calculated by multiplying one transformation with the inverse of the other,

$$ T_{\mathrm{diff},k} = {}^{\mathrm{P}}T_{\mathrm{D},k}\,({}^{\mathrm{P}}T_{\mathrm{D,mod},k})^{-1}, $$

and is split into a rotation $R_{\mathrm{diff},k} \in \mathrm{SO3}$ and a translation $t_{\mathrm{diff},k} \in \mathbb{R}^3$:

$$ \begin{pmatrix} R_{\mathrm{diff},k} & t_{\mathrm{diff},k} \\ 0_{1\times3} & 1 \end{pmatrix} $$

From these, the rotational residual $r_{\mathrm{r},k}$ and the translational residual $r_{\mathrm{t},k}$ are calculated:

$$ r_{\mathrm{r},k} = \mathrm{angle}(R_{\mathrm{diff},k}) \text{ and } r_{\mathrm{t},k} = ||t_{\mathrm{diff},k}||, $$

where the angle of the rotation is calculated from the trace of the rotation matrix, i.e., from the sum of diagonal elements [12]:

$$ \mathrm{angle(R)} = \arccos\left(\frac{1}{2}[\mathrm{trace}(R) - 1]\right). $$

The optimal axis positions ${}^{\mathrm{P}}p_{\mathrm{a1,opt}}$ and ${}^{\mathrm{P}}p_{\mathrm{a2,opt}}$, the optimal axis orientations ${}^{\mathrm{P}}a_{1,\mathrm{opt}}$ and ${}^{\mathrm{P}}a_{2,\mathrm{opt}}$ and the optimal joint angles $Q_{1,\mathrm{opt}} = (q_{11,\mathrm{opt}}, \ldots, q_{1n_{\mathrm{p}},\mathrm{opt}})$ and $Q_{2,\mathrm{opt}} = (q_{21,\mathrm{opt}}, \ldots, q_{2n_{\mathrm{p}},\mathrm{opt}})$ are identified by minimising the mean weighted sum of rotational and translational residuals:

$$ ({}^{\mathrm{P}}p_{\mathrm{a1,opt}},\, {}^{\mathrm{P}}a_{1,\mathrm{opt}},\, Q_{1,\mathrm{opt}}) = \underset{{}^{\mathrm{P}}p_{\mathrm{a1}},\, {}^{\mathrm{P}}a_1,\, Q_1}{\mathrm{argmin}} \\ \frac{1}{n_{\mathrm{p}}} \sum_{k=1}^{n_{\mathrm{p}}} w_{\mathrm{r}}\, r_{\mathrm{r},k}({}^{\mathrm{P}}a_1,\, q_{1k}) + w_{\mathrm{t}}\, r_{\mathrm{t},k}({}^{\mathrm{P}}p_{\mathrm{a1}},\, {}^{\mathrm{P}}a_1,\, q_{1k}) $$

and

$$ ({}^{\mathrm{P}}p_{\mathrm{a1,opt}},\, {}^{\mathrm{P}}p_{\mathrm{a2,opt}},\, {}^{\mathrm{P}}a_{1,\mathrm{opt}},\, {}^{\mathrm{P}}a_{2,\mathrm{opt}},\, Q_{1,\mathrm{opt}},\, Q_{2,\mathrm{opt}}) = \\ \underset{{}^{\mathrm{P}}p_{\mathrm{a1}},\, {}^{\mathrm{P}}p_{\mathrm{a2}},\, {}^{\mathrm{P}}a_1,\, {}^{\mathrm{P}}a_2,\, Q_1,\, Q_2}{\mathrm{argmin}} \frac{1}{n_{\mathrm{p}}} \sum_{k=1}^{n_{\mathrm{p}}} \Big(w_{\mathrm{r}}\, r_{\mathrm{r},k}({}^{\mathrm{P}}a_1,\, {}^{\mathrm{P}}a_2,\, q_{1k},\, q_{2k}) \quad + \\ w_{\mathrm{t}}\, r_{\mathrm{t},k}({}^{\mathrm{P}}p_{\mathrm{a1}},\, {}^{\mathrm{P}}p_{\mathrm{a2}},\, {}^{\mathrm{P}}a_1,\, {}^{\mathrm{P}}a_2,\, q_{1k},\, q_{2k}) \Big), $$

respectively.

We choose the following values for the weights w_{r} and w_{t}:

$$ w_{\mathrm{r}} = 1\,\mathrm{deg}^{-1}, \\ w_{\mathrm{t}} = 1\,\mathrm{mm}^{-1}. $$

Note that the optimisation can be accelerated by optimising the joint angles q_{1k} and q_{2k}, respectively, in a nested optimisation in each iteration of the position and orientation optimisation, especially if n_{p} is large. We use this nested optimisation approach with the simplex algorithm by Nelder and Mead [13], as implemented in the Matlab *fminsearch* function.

C. Compensation of skin movement

In order to compensate the STA, the skin movement is modelled as described in Sec. II-D. The model states that the skin marker rotates around the same rotation axis or axes as the adjacent bone, albeit with a smaller rotation angle that is proportional to the bone rotation angle.

The PIP and DIP joints are modelled with one degree of freedom (DoF):

$$\begin{pmatrix} {}^{\mathrm{P}}p_{\mathrm{m,mod},k} \\ 1 \end{pmatrix} = \mathrm{rot}_{4\times4}\left({}^{\mathrm{P}}p_{\mathrm{a1}},\, {}^{\mathrm{P}}a_1,\, c_1\, q_{1k}\right) \begin{pmatrix} {}^{\mathrm{P}}p_{\mathrm{m0}} \\ 1 \end{pmatrix},$$

and the MCP joints are modelled with two DoF:

$$\begin{pmatrix} {}^{\mathrm{P}}p_{\mathrm{m,mod},k} \\ 1 \end{pmatrix} = \mathrm{rot}_{4\times4}\left({}^{\mathrm{P}}p_{\mathrm{a1}},\, {}^{\mathrm{P}}a_1,\, c_1\, q_{1k}\right) \mathrm{rot}_{4\times4}\left({}^{\mathrm{P}}p_{\mathrm{a2}},\, {}^{\mathrm{P}}a_2,\, c_2\, q_{2k}\right) \begin{pmatrix} {}^{\mathrm{P}}p_{\mathrm{m0}} \\ 1 \end{pmatrix},$$

where ${}^{\mathrm{P}}p_{\mathrm{m,mod},k}$ is the modelled marker position in posture k,
${}^{\mathrm{P}}p_{\mathrm{a1}}$ is a point on the first rotation axis,
${}^{\mathrm{P}}a_1$ is the Cartesian orientation of the first rotation axis,
c_1 is the skin movement proportionality factor for the first rotation axis,
q_1k is the bone rotation angle around the first rotation axis,
${}^{\mathrm{P}}p_{\mathrm{a2}}$ is the a point on the second rotation axis,
${}^{\mathrm{P}}a_2$ is the Cartesian orientation of the second rotation axis,
c_2 is the skin movement proportionality factor for the second rotation axis, and
q_2k is the bone rotation angle around the second rotation axis.

The amount $s_{\mathrm{residual},k}$ of residual STA is calculated as the distance between the modelled marker position and the measured marker postition:

$$s_{\mathrm{residual},k} = ||{}^{\mathrm{P}}p_{\mathrm{m},k} - {}^{\mathrm{P}}p_{\mathrm{m,mod},k}||.$$

As described in Sec. II-D, the initial marker position ${}^{\mathrm{P}}p_{\mathrm{m0}}$ and the proportionality factors c_1 and c_2 can be optimised to best describe the skin movement. As a starting point, the initial marker position is assumed to be equal to the marker position in the reference posture, and the proportionality factors are assumed to be 0.5:

$$\begin{aligned} {}^{\mathrm{P}}p_{\mathrm{m0,start}} &= {}^{\mathrm{P}}p_{\mathrm{m,ref}}, \\ c_{1,\mathrm{start}} &= 0.5, \\ c_{2,\mathrm{start}} &= 0.5. \end{aligned}$$

The mean amount of residual STA at the starting point and its standard deviation over all postures is shown in the third column of Table I.

The optimal skin movement parameters ${}^{\mathrm{P}}p_{\mathrm{m0,opt}}$, $c_{1,\mathrm{opt}}$ and $c_{2,\mathrm{opt}}$ minimise the mean amount of residual STA over all postures:

$$\left[{}^{\mathrm{P}}p_{\mathrm{m0,opt}},\, c_{1,\mathrm{opt}},\, c_{2,\mathrm{opt}}\right] = \underset{{}^{\mathrm{P}}p_{\mathrm{m0}},\, c_1,\, c_2}{\mathrm{argmin}} \frac{1}{n_{\mathrm{p}}} \sum_{k=1}^{n_{\mathrm{p}}} s_{\mathrm{residual},k}({}^{\mathrm{P}}p_{\mathrm{m0}},\, c_1,\, c_2), \quad (16)$$

joint name	mean STA (mm) ± SD uncompensated	default values	optimised values	cross-validated	optimised parameters c1	c2
MCP1	3.2 ±2.6	2.3 ±1.5	2.0 ±1.4	2.5 ±1.5	0.5	0.4
MCP2	6.8 ±4.0	3.7 ±2.3	3.2 ±1.7	3.7 ±1.7	0.5	0.8
PIP2	2.5 ±3.3	1.4 ±1.0	0.8 ±0.4	1.1 ±0.6	0.8	
DIP2	1.7 ±1.9	1.1 ±0.6	0.9 ±0.4	1.1 ±0.5	0.6	
MCP3	6.6 ±5.0	2.8 ±2.1	2.0 ±1.2	2.2 ±1.3	0.6	1.2
PIP3	3.6 ±4.4	1.7 ±1.1	1.4 ±0.9	1.6 ±0.9	0.6	
DIP3	1.7 ±1.6	1.7 ±1.2	1.2 ±0.9	1.1 ±0.9	0.4	
MCP4	7.2 ±5.4	3.1 ±2.5	2.0 ±1.3	2.4 ±1.2	0.8	0.7
PIP4	3.0 ±3.6	1.7 ±1.2	1.5 ±1.1	1.6 ±1.2	0.6	
DIP4	1.7 ±1.7	1.2 ±0.8	1.0 ±0.7	1.1 ±0.7	0.6	
MCP5	6.9 ±4.5	4.6 ±2.4	2.8 ±1.6	3.5 ±1.8	0.5	0.2
PIP5	2.9 ±3.1	2.3 ±1.4	1.7 ±1.2	1.9 ±1.3	0.7	
DIP5	2.1 ±1.7	1.7 ±1.1	1.3 ±1.0	1.4 ±1.0	0.7	
mean	3.8 ±3.3	2.3 ±1.5	1.7 ±1.1	1.9 ±1.1		

TABLE I: Validation of the skin movement model using MRI measurement as ground thruth. The second to fifth columns show the mean and standard deviation over all postures of the amount of STA – uncompensated, compensated with default parameters, compensated with optimised parameters and compensated with optimised parameters in a leave-one-out cross-validation. The sixth and seventh column show the optimised values of the skin movement proportionality factors.

where n_{p} is the number of postures. The simplex algorith by Nelder and Mead [13], as implemented in Matlab, is used to find the optimal parameters.

The mean amount of residual STA using the optimised parameters and its standard deviation over all postures, as well as the values of the optimal proportionality factors are shown in the fourth, sixth and seventh column of Table I, respectively.

A leave-one-out cross-validation is performed to check against overfitting of the data. For this, the skin movement parameters are optimised according to Eq. 16, using all postures except one ("training set"). The residual STA is calculated for the omitted hand posture ("test set"). This procedure is repeated n_{p} times, each time omitting another posture from the training set.

The mean and standard deviation of the cross-validated amounts of residual STA are shown in column five of Table I.

The results show that the measured reference marker position is a good starting point for the initial marker position and that 0.5 is a good starting point for the proportionality factor: modelling the skin movement with these values already reduces the amount of STA of the investigated subject on average from 3.8 to 2.3 mm. Still, optimising the parameters is useful, further reducing the STA to 1.7 mm. The cross-validated residual is only slightly higher than the optimised residual; i.e., the parameters generalise well on unknown joint postures.

IV. Calibration of subject-specific static parameters

When regarding hand movement over time, some properties of the hand change while other properties are static. For example, when modelling the joints of the fingers as simple rotation axes, the positions and orientations of the axes in a

reference posture are static, while the rotation angles around these axes vary during the movement. There are additional static parameters when skin movement is modelled in addition to bone movement.

In order to reconstruct realistic values of the joint angles from marker data, the kinematic model employed should mimic as closely as possible the actual kinematics of the subject being recorded. Once the *optimal* topology of the kinematic model has been selected [11], this amounts to identifying (i) the subject specific geometric parameters a_G, related to the positions and orientations of the joint axes, which affect the twist coordinates ξ_{ik}, and (ii) the parameters a_B and a_J controlling the location of the *bone* and the *joint* markers, respectively, with respect to the hand kinematic structure. It is worth noting that the parameters defining the skin compensation mechanisms in eq. (12) are elements of a_J and are treated like all the other parameters.

Let y_k denote the vector containing the coordinates of all the markers measured by the Motion Capture system at time instant k. Moreover, let $f(x_k; a_G, a_B, a_J)$ represent the corresponding coordinates when the joint angle values are set to x_k and the static parameters are set to the values a_G, a_B and a_J. At time instant k it is possible to define the residual

$$r_k = r(x_k; a_G, a_B, a_J) := y_k - f(x_k; a_G, a_B, a_J), \quad (17)$$

expressing the instantaneous misfit between measurements and estimates provided by the model. By considering a number N_p of *training* hand postures it is convenient to cast all the corresponding residuals in a unique vector R as follows

$$R(x; a_G, a_B, a_J) := [r_1^T \; r_2^T \; \cdots r_k^T \; \cdots r_{N_p}^T]^T, \quad (18)$$

and set $x = [x_1^T \; x_2^T \; \cdots x_{N_p}^T]^T$, such that the following cost function, that is a *scalar* measure of misfit, can be introduced

$$g(x; a_G, a_B, a_J) := \frac{1}{2} R^T R = \frac{1}{2} \sum_{k=1}^{N_p} r_k^T r_k \quad (19)$$

At this point, the calibration of the skeletal and marker parameters can be framed as the following *constrained least-squares minimization* problem

$$(x^*; a_G^*, a_B^*, a_J^*) = \underset{\substack{x_k \in \mathcal{D}_x \\ a \in \mathcal{D}_a}}{\operatorname{argmin}} \; g(x; a_G, a_B, a_J), \quad (20)$$

where $\mathcal{D}_x$ represents a feasibility region for the generic value x_k of joint angles at instant k, and $a \in \mathcal{D}_a$ can be expanded as $a_G \in \mathcal{D}_{a_G}$, $a_B \in \mathcal{D}_{a_B}$ and $a_J \in \mathcal{D}_{a_J}$. It is important to observe that all the above requirements can be written explicitly as *box constraints*, e.g. $x_k \in \mathcal{D}_x \iff l_k \preceq x_k \preceq u_b$, where l_k and u_k are physiological joint angle bounds for the hand that can be recovered from [14]. The other regions $\mathcal{D}_{a_g}, \mathcal{D}_{a_B}$ and $\mathcal{D}_{a_J}$ can be defined as tolerance regions around nominal and/or most likely values. These that can be estimated through direct measurements, e.g. with a caliper, and can be employed as *initial guesses* of the numerical minimization procedure. In our implementation, the solution of problem (20) is obtained employing a *primal-dual interior point method* based on [15].

It is worth observing that, besides the optimal values of the skeletal and marker associated parameters a_G^* and a_B^*, a_J^*, respectively, the solution of (20) provides, as a *costly by product*, the optimal joint angles values x^* corresponding to the N_p training poses. Even if these values are actually discarded, since their values for a continuous movement is found as described in Sec. V, their inclusion as variables in (20) is an obliged stage, since no a priori informed estimate can be made on joint angle values corresponding to a given hand posture.

V. Posture reconstruction

The problem of computing joint angle values given marker coordinates is sometimes tackled as one of *inverse kinematics*. However, if uncertainty in the model description and noisy measurements are to be treated as intrinsic features and not as an afterthought, it is more appropriate to cast the problem in the general framework of *probabilistic inference*.

Let x denote the vector of all latent variables in the model. In our analysis x represent joint angles, and x_k denote their values at time instant k. Geometric parameters a_G, bone marker parameters a_B and joint marker parameters a_J are considered as known from the previously described calibration procedure, and their values will not change during the posture reconstruction process.

Let then y denote the vector obtained by casting the coordinates of all markers measured by the Motion Capture system, and let y_k represent their values at time instant k. The objective of our analysis is to estimate the most likely state $\hat{x}_{k+1|k+1}$, and its confidence interval in the form of a covariance matrix $P_{k+1|k+1}$, given the measurements up to time instant $k+1$ as well as prior information $\hat{x}_{k|k}$. The notation here used is standard in probabilistic inference and it is based on [16].

The two pillars of probabilistic inference are: (i) the *process model* and (ii) the *observation model*. In our case, the process model, i.e. the model describing the state transition is unknown with no controlled inputs, since only the kinematics of movement is considered. Therefore, modeling noise v_k at instant k as a Gaussian process with zero mean and covariance V_k, we can describe the process model as a *random walk* in the state

$$x_{k+1} = x_k + v_k, \quad v_k \sim \mathcal{N}_v(0; V_k) \quad (21)$$

The observation model, relating the latent state x_k and the measurements y_k, both at time instant k, is given by the *direct kinematics* relationship

$$y_k = f(x_k) + w_k, \quad w_k \sim \mathcal{N}_w(0; W_k) \quad (22)$$

The misfit between marker coordinates measured by the motion tracking system and estimates provided by the direct kinematics are modeled as a Gaussian process with zero mean and covariance W_k. Therefore, introducing the notion of residual $r(y, x) := y - f(x)$, it is possible to write, at time instant k,

$$r(y_k, x_k) = y_k - f(x_k) = w_k, \quad r_k \sim \mathcal{N}_r(0; W_k) \quad (23)$$

By differentiating eq. (23), the equation relating the Jacobian of the residual $J_r(x)$ and the kinematic (positional) Jacobian

$J_f(x)$ is obtained

$$J_r(x) = -J_f(x). \tag{24}$$

Since $J_f(x)$ can be composed using the elemental *hybrid Jacobians* $J_{BM_{ij}}^{B,[O_{M_{ij}}]}$, computed as in (7), for all the markers, eq. (24) provides an closed-form solution to the computation of the important matrix $J_r(x)$.

The *recursive estimation* procedure is based on a *iterative* Extended Kalman Filter (EKF) described as follows. Starting from an initial estimate $\hat{x}_{k|k}$, with state covariance $P_{k|k}$, the *prediction step*, based on the linear process dynamics (21), produces

$$\hat{x}_{k+1|k} = \hat{x}_{k|k}, \tag{25}$$

$$P_{k+1|k} = P_{k|k} + V_k \tag{26}$$

Therefore, the *prior* density over the latent variable space is

$$p(x_{k+1}|y_{1:k}) = \mathcal{N}_x(\hat{x}_{k+1|k}; P_{k+1|k}), \tag{27}$$

which includes measurements only up to y_k. The subsequent *correction step* is based on the maximization of the *posterior* density $p(x_{k+1}|y_{1:k+1})$ obtained when also y_{k+1} is included. This density, up to a *normalizer in Bayes rule* η, can be written as

$$p(x_{k+1}|y_{1:k+1}) = \eta\, \mathcal{N}_r(0; W_k)\mathcal{N}_x(\hat{x}_{k+1|k}; P_{k+1|k}) \tag{28}$$

The *maximum a posteriori* estimate $\hat{x}_{k+1|k+1}$ is the value of x_{k+1} which maximizes the above expression for given y_{k+1} (contained in r_{k+1}) and $x_{k+1|k}$. By denoting for clarity the sought for value $\hat{x}_{k+1|k+1}$ simply with x, the maximization of (28) is equivalent to minimizing w.r.t. x the function $-\log(p(x|y_{1:k+1}))$ which, up to an additive constant, is

$$\begin{aligned} h(x) = &\frac{1}{2} r^T(y_{k+1}, x) W_{k+1}^{-1} r(y_{k+1}, x) + \\ &+ \frac{1}{2}(x - \hat{x}_{k+1|k})^T P_{k+1|k}^{-1}(x - \hat{x}_{k+1|k}) \end{aligned} \tag{29}$$

It is worth noting that function $h(x)$ plays the role of a cost function where the first term encourages *explaining the measurements* from the motion tracking system, while the second term suggests *staying close to the prior* which, due to (21), is the solution at the preceding time step, thus avoiding motion discontinuities. Due to the nonlinearity of the residual $r(y_{k+1}, x)$ w.r.t. x, caused by the nonlinearity of the direct kinematics model $f(x)$, the minimization of (29) leads to a *nonlinear least-squares problem*. This problem can be easily handled by modern *trust-region* methods [17], [18]. These methods progressively minimize (29) by iteratively minimizing quadratic models of it built at each step and following a policy of acceptance/rejection of the step based on the agreement between the reduction in the nonlinear function and its approximant.

It is worth noting that, at each step of the method (inner loop of the numerical method of minimization) the Gauss-Newton step is calculated as

$$s = -H(x)^{-1}\nabla(x), \tag{30}$$

where the *gradient* vector $\nabla(x)$ and the *Hessian* matrix $H(x)$ are

$$\nabla(x) = J_r(x)^T W_{k+1}^{-1} r(y_{k+1}, x) + P_{k+1|k}^{-1}(x - \hat{x}_{k+1|k}) \tag{31}$$

$$H(x) = J_r(x)^T W_{k+1}^{-1} J_r(x) + P_{k+1|k}^{-1} \tag{32}$$

It can be proved that the posterior covariance $P_{k+1|k+1} = H(\hat{x}_{k+1|k+1})$, that is the Hessian evaluated at the MAP solution.

It is worth observing that the EKF is a special case of our *iterative* EKF, corresponding to a single step taken in the minimization of $h(x)$ in eq. (29). In fact, the EKF performs a linearization of the residual $r(y_{k+1}, x)$, thus obtaining already a quadratic model of $h(x)$, which converges in one iteration. However, while in the KF the residual is actually linear and the above procedure is optimal, the EKF, neglecting $O(\|x\|^2)$ terms in the observation model, can lead to inaccurate results. It is therefore advisable to employ the *iterative* EKF to improve accuracy through additional iterations until convergence and/or as long as the computational effort is acceptable.

VI. Experiments and Results

The models and techniques described in the previous sections have been used to reconstruct hand poses in experiments conducted by subjects with an optical tracking system. These techniques should be thought as tools to improve hand pose reconstruction since they allow to take into account differences in hand shape and dimensions, skin movement, as well as to vary the number of DoFs used for the kinematic hand model in use. The latter aspect, for example, enables to face the study of synergies and their dependency on kinematic model dimension. More specifically, although a complete movement can be reconstructed, we focus on "static" grasping poses. To analyze reconstruction outcomes, we consider, respectively, only 24 out of 26 DoFs of the kinematic model previously described (wrist DoFs are neglected) and only 15 DoFs, chosen as in [6]; Principal Component Analysis (PCA) has been performed for both cases and Principal Components (PCs, or synergies) obtained and results are compared with the ones presented in [6]. In [6] authors first analyzed hand postural synergies [1] for grasping by means of PCA. In this work, authors focused on central contributions to hand posture modulation, analyzing a large number of different imagined grasped objects, thus avoiding any mechanical interference as it would result from the contact with real elements. They demonstrated that only a few linear combinations of hand DoFs (in this case a 15 DoF kinematic model was considered) is sufficient to take into account most of the variance in the set.

A. Materials and Methods

1) Experimental task: Subjects were instructed to shape their right hand as to grasp a certain amount of objects ($n = 20$, Table II) which were not physically present during the experiment. Pictures of the objects were instead shown on a computer screen, and the subject was asked to grasp them as

1. Bucket	11. Hammer
2. Calculator	12. Ice cube
3. Chalk	13. Jar lid
4. Cherry	14. Light bulb
5. Computer mouse	15. Pen
6. Dinner plate	16. Rope
7. Espresso cup	17. Telephone handset
8. Fishing rod	18. Tennis racket
9. Frisbee	19. Toothpick
10. Hair dryer	20. Wrench

TABLE II: List of objects used in the task

if they want to use them in a specific, priorly agreed upon way.

The subject was asked to imagine the object floating in space at a distance of about $10-20$ cm ahead of the subject's frontal plane, in the same configuration which was shown in the picture. The subject was seated on a chair, and their forearm rested on the armrest. While waiting at the rest position, the subject was asked to keep their hand in a position as "flat" as possible. When they reached the grasp configuration, they were asked to wait a few seconds before coming back to the rest position again. Each subject performed a total of six trials for each of the objects; all trials were presented in random order. These six trials were preceded by a few training trials, in order for them to be familiar with all the pictures presented.

Four right-handed subjects (two males and two females, age in the interval 20 to 30 years) participated in this study. All subjects gave informed consent, and the protocols were approved by the ethical committee of the University of Pisa.

A single trial was timed as follows:

- at first, the picture of one object was shown for 3 seconds
- then, after removing the picture, the subject waited 2 seconds before hearing a "beep" sound
- when they heard the beep, they moved to perform the grasp, stopped at the final configuration for a few seconds, and then came back
- the whole cycle (between the presentation on the screen of two consecutive objects) lasted 12 seconds.

B. Experimental Procedure and Data Analysis

Hand posture was obtained with the identification procedure described in Section V, measuring the position of optical markers using an optical motion capture system (Phase Space, San Leandro, CA – USA) composed of 10 stereo-cameras at 480 Hz, undersampling in post-processing down to 15 Hz and then smoothing the reconstructed postural angles with a 5 samples moving average filter. Subsequently, a selection of the actual frame to consider for a specific grasp has been carried out, based on the timing of object pictures presentation, via visual inspection.

The protocol for marker placement is as follows (see Figure 4 for an illustration):

- a rapid prototyping plastic bracelet strapped on the wrist in order to obtain a local (proximal) frame of the hand at each time step
- one marker is placed on each "bone" as considered in the model of Section II
- one marker is placed on each "joint" in the following list:
  - Thumb: carpometacarpal (CMC), metacarpo-phalangeal (MCP), inter-phalangeal (IP)
  - Index: MCP, proximal-inter-phalangeal (PIP)
  - Middle: MCP, PIP
  - Ring: PIP
  - Little: PIP

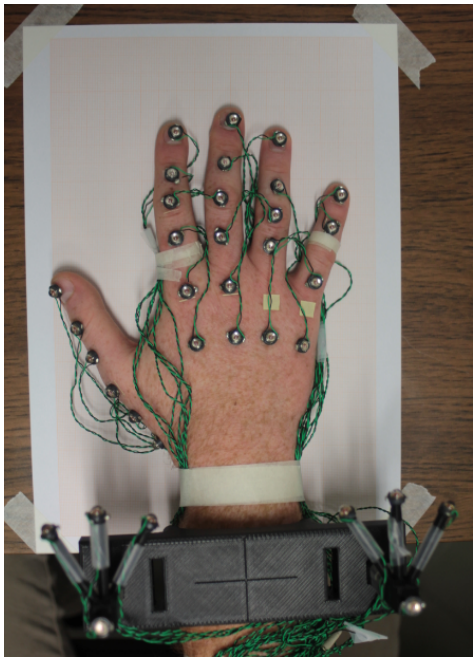

Fig. 4: The hand of one subject after all markers have been placed, showing the protocol for marker placement.

1) Data Analysis: Let consider first the analysis with the model with 15 DoFs. In this case the percentage of variance accounted for by each principal component (table III) and the cumulative variance (table IV) are similar to the values reported in [6]. Of course differences between subjects can occur (see e.g. subject T.C.). The values we obtained are slightly smaller compared to [6], possibly because we do not reduce intra-object variability thus considering all the repetitions for each object grasp in data analysis. However the main result is that with only three synergies $\sim 80\%$ of data variance is taken into account for all subjects (except for T.C.), thus suggesting a reduction of the 15 DoFs to be recorded: in other terms, since synergies express the constraints in inter-digit movement due to both peripheral and central factors [1], the dimensionality of the DoFs that can be independently controlled by the nervous system is smaller than the one due to purely mechanical kinematic space [19]. Considering the covariation matrix as reported in Figure 5, what is noticeable is that MCP (MetaCarpo-Phalangeal) angles of adjacent fingers as well the PIP (Proximal-Interphalangeal)angles are highly related to each other, with the extent of correlation decreasing with the separation between pairs of fingers. This result is comparable to the one in [6]. Same considerations can be drawn for the 24 DoF covariation matrix, as it is reported

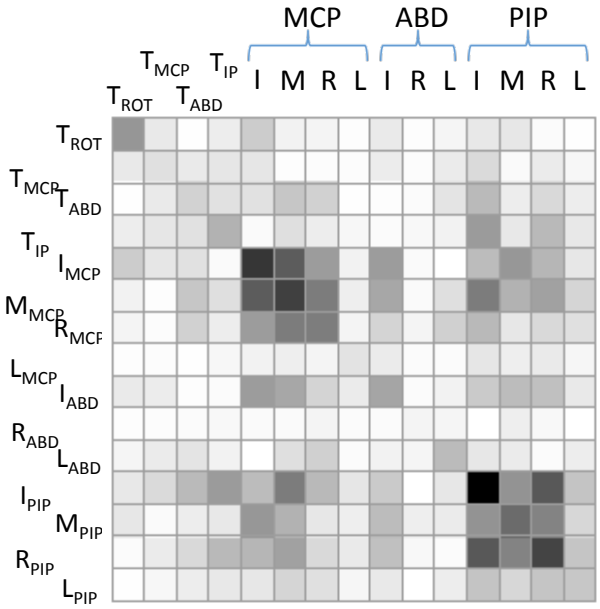

Fig. 5: Gray scale plot of the covariance matrices for all subjects analyzing 15 DoFs. For sake of clarity and to enhance result comparison, the same naming in [6] is adopted; the term ABD refers to the adduction/abduction degrees of freedom, MCP to metacarpo-phalangeal joints, PIP to the proximal-interphalangeal joints, DIP to distal-interphalangeal joints.

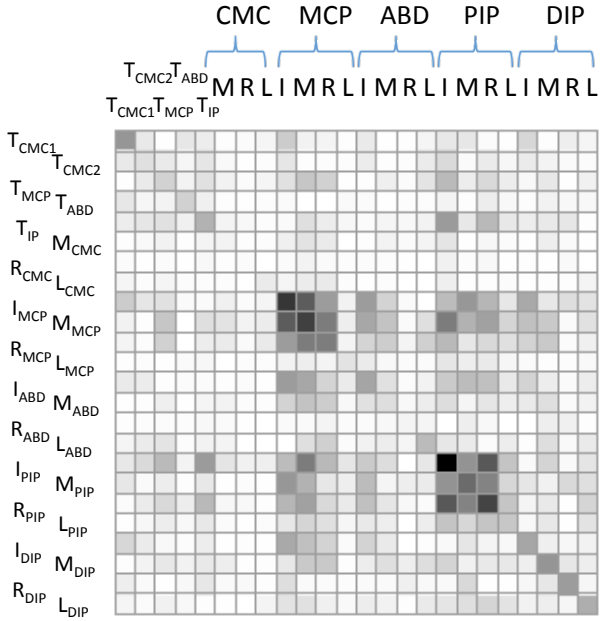

Fig. 6: Gray scale plot of the covariance matrices for all subjects analyzing 24 DoFs. Gray scale plot of the covariance matrices for all subjects analyzing 15 DoFs. For sake of clarity and to enhance result comparison, the same naming in [6] is adopted; the term ABD refers to the adduction/abduction degrees of freedom, MCP to metacarpo-phalangeal joints, PIP to the proximal-interphalangeal joints, DIP to distal-interphalangeal joints.

in Figure 6. In this case, as expected, the $\sim 80\%$ of data variance is taken into account with more synergies, more specifically with five synergies (except for T.C.) – cf. table V and table VI; however, the proportion of effective DoFs (as it results from the number of the synergies engaged to get $\sim 80\%$ of data variance accounted for) and the number of DoFs used to describe the kinematic model is pretty the same of the one observed for the 15 DoF case. In Figure 8 and Figure 10 the distribution of the angular differences for all joint angles between hand posture reconstructed from the first two PCs in 15 and 24 DoFs, respectively, and the actual posture recorded; in both cases, for a large percentage of poses ($> 70\%$), the angular difference in degrees is within ± 5. This result suggests that, although with the differences due to the kinematic model in use, the first two PCs are the most important for the reconstruction. This can be also observed from Figure 7 and Figure 9, where the distribution of normalized amplitudes of the first five PCs for 24 and 15 DoF models are reported, respectively. The amplitudes are normalized to the maximum (absolute) value of the first PC. Notice that the amplitude to the third through the fifth PCs are uniformly small, although they contribute to the variance accounted for (this fact is especially true for the 24 DoF model). All these results are coherent with the one reported in [6]. Finally, in Figure 11, postural synergies defined by the first two principal components in 24 DoFs are reported. The central hand posture is the average over 120 postures (20 different objects 6 times each) for one subject (A.C.). The postures to the *right* and *left* are for the maximum and minimum values of the first principal component (*PC1*), while other principal components have been set to zero. The postures at the *top* and *bottom* are the same for the second principal component (*PC2*). As in [6], along the PC1 (horizontal) axis, it is possible to observe a gradual closure of the end: at one extreme, it is noticeable an extension and abduction of the fingers at the MCP joint (PC1 max), while at the other extreme, MCP joint flexion and adduction is observed (PC1 min). Along the PC2 (vertical) axis, with PIP joint flexion and MCP joint extension while moving toward PC2 min. The thumb abduction and internal rotation decrease towards PC2 max. This result suggests that the model of synergy still works in spite of the dimension of the kinematic model in use, with many similarities across models with a different number of DoFs.

Subjects	PC_1	PC_2	PC_3	PC_4	PC_5
AC	67.1	13.5	7.2	2.8	2.5
MB	48.9	18.1	12.9	5.2	3.7
TC	32.7	20.6	12.0	8.6	7.4
DR	57.3	13.9	10.7	4.1	3.3

TABLE III: Percent variance accounted for by each principal component in 15 DoFs

Subjects	PC_1	PC_2	PC_3	PC_4	PC_5
AC	67.1	80.6	87.7	90.5	93.0
MB	48.9	67.0	79.9	85.1	88.8
TC	32.7	53.3	65.3	73.9	81.3
DR	57.3	71.2	81.9	86.0	89.3

TABLE IV: Cumulative percent variance accounted for by 15 DoFs PCs

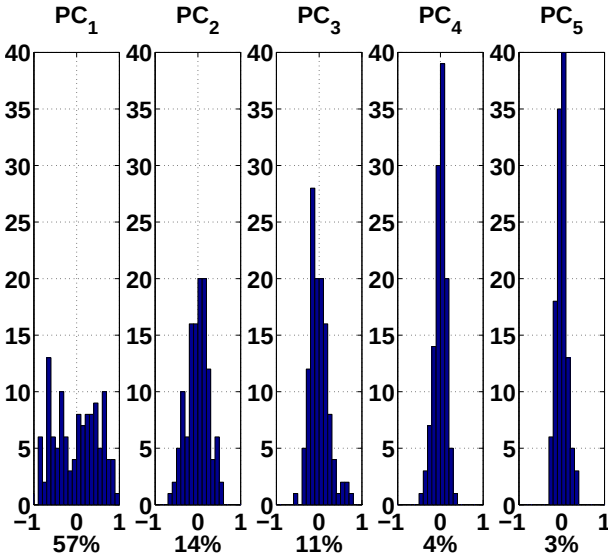

Fig. 7: Distribution of normalized amplitudes of the first five principal components in 15 DoFs. These amplitudes have been normalized to the maximum (absolute) value of the first PC. The data shown are for one subject (D.R.).

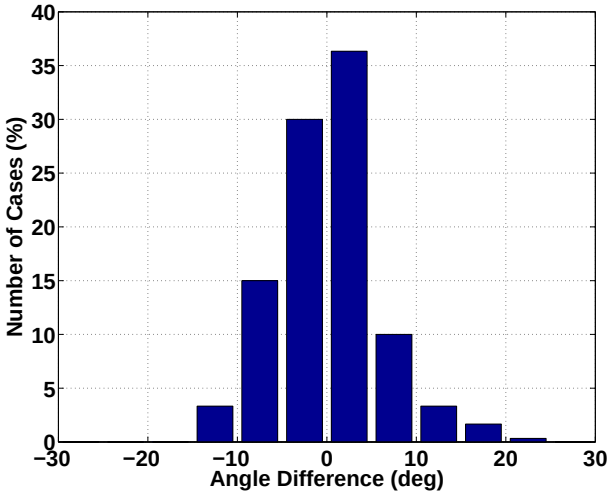

Fig. 8: Distribution of the angular differences for all joint angles between hand posture reconstructed from the first 2 PCs in 15 DoFs and the actual posture recorded. The data are for all objects from one subject (D.R.).

Subjects	PC_1	PC_2	PC_3	PC_4	PC_5
AC	55.6	13.2	7.3	5.3	4.5
MB	40.0	16.1	12.3	5.9	5.2
TC	27.9	17.3	12.1	7.4	6.3
DR	45.7	13.6	9.4	7.4	5.0

TABLE V: Percent variance accounted for by each principal component in 24 DoFs

VII. Conclusions and Future Work

In this work a complete procedure to reconstruct human hand posture is presented The kinematic hand model in use is fully parameterized and it allows to take into account differences in subject hands. Furthermore, the introduction of a soft-tissue artifact compensation mechanism makes the procedure amenable of in-vivo to joint angle recordings via optical tracking of markers attached to the skin. The parametrization structure of the model has then been exploited to reconstruct hand poses in experiments, aiming at analyzing postural synergies in grasping, using kinematic models with a different number of degrees of freedom. Results are compared to the ones reported in [6], showing a significant coherence in the synergies obtained, independently form the dimensionality of the kinematic description in use. In conclusion, this paper offers a useful tools that can be used to investigate more in depth and with more accuracy the synergy concept; the final results, after the definition of meaningful mapping strategy, might drive the definition of robotic hand postures able to realize effective grasps, or be used as *a priori* information for hand avatar animation [20] or for the improvement of the design and the performance of glove-based Hand Pose Reconstruction (HPR) systems [21], [22].

Subjects	PC_1	PC_2	PC_3	PC_4	PC_5
AC	55.6	68.7	76.1	81.3	85.8
MB	40.0	56.1	68.4	74.3	79.5
TC	27.9	45.3	57.4	64.8	71.1
DR	45.7	59.3	68.7	76.1	81.1

TABLE VI: Cumulative percent variance accounted for by 24 DoFs PCs

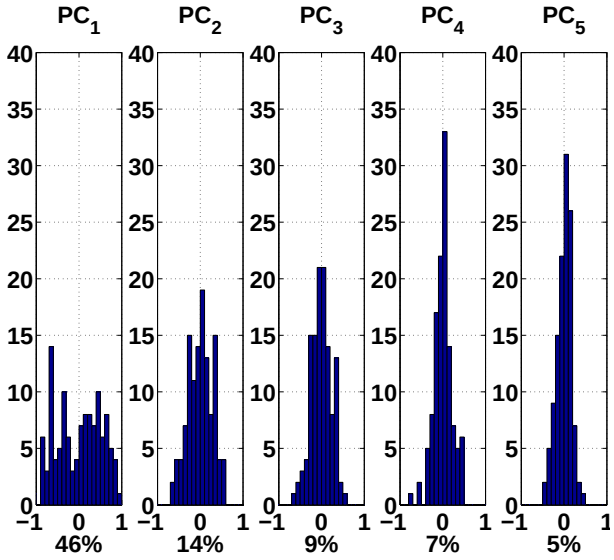

Fig. 9: Distribution of normalized amplitudes of the first five principal components in 24 DoFs. These amplitudes have been normalized to the maximum (absolute) value of the first PC. The data shown are for one subject (D.R.).

References

[1] M. H. Schieber and M. Santello, "Hand function: peripheral and central constraints on performance," *Journal of Applied Physiology*, vol. 96, no. 6, pp. 2293 – 2300, 2004.

[2] A. Gustus, G. Stillfried, J. Visser, and H. Jörntell, "Human hand modelling: kinematics, dynamics, applications," *Biological Cybernetics*, vol. 106, pp. 741–755, 2012. [Online]. Available: http://dx.doi.org/10.1007/s00422-012-0532-4

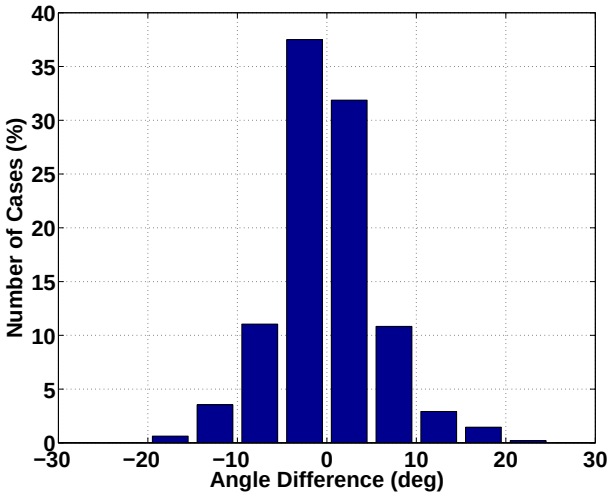

Fig. 10: Distribution of the angular differences for all joint angles between hand posture reconstructed from the first 2 PCs in 24 DoFs and the actual posture recorded. The data are for all objects from one subject (D.R.).

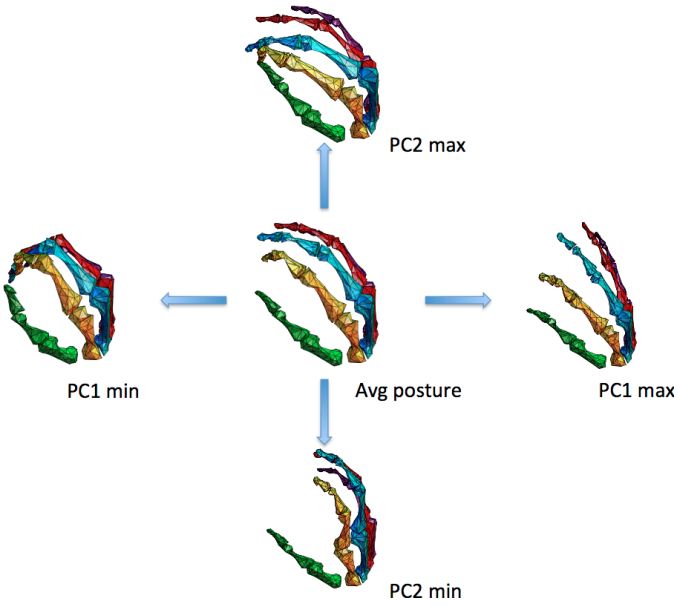

Fig. 11: Postural synergies defined by the first two principal components. The central hand posture is the average over 120 postures (20 different objects 6 times each) for one subject (A.C.). The postures to the *right* and *left* are for the maximum and minimum values of the first principal component (*PC1*), while other principal components have been set to zero. The postures at the *top* and *bottom* are the same for the second principal component (*PC2*).

[3] X. Zhang, L. Sang-Wook, and P. Braido, "Determining finger segmental centers of rotation in flexion-extension based on surface marker measurement," *Journal of Biomechanics*, vol. 36, pp. 1097–1102, 2003.

[4] R. M. Murray, Z. Li, and S. Sastry, *A Mathematical Introduction to Robotic Manipulation*. Boca Raton, FL: CRC Press, 1994.

[5] K. Waldron and J. Schmiedeler, *Handbook of Robotics*. Springer, 2008, ch. Kinematics, pp. 9–34.

[6] M. Santello, M. Flanders, and J. F. Soechting, "Postural hand synergies for tool use," *The Journal of Neuroscience*, vol. 18, no. 23, pp. 10 105 – 10 115, 1998.

[7] R. W. Brockett, "Robotic manipulators and the product of exponentials formula," in *Mathematical Theory of Networks and Systems*, P. A. Fuhrman, Ed. New York: Springer-Verlag, 1984.

[8] M. Gabiccini, "A twist exponential approach to gear generation with general spatial motions," *Mechanism and Machine Theory*, vol. 44, no. 2, pp. 382–400, 2009.

[9] G. Wu, C. T. van der Helm, H. E. J. Veeger, *et al.*, "ISB recommendation of joint coordinate systems of various joints for the reporting of human joint motion - part ii: shoulder, elbow, wrist and hand," *Journal of Biomechanics*, vol. 38, pp. 981–992, 2005.

[10] U. Hillenbrand, "Pose clustering from stereo data," in *Proceedings VISAPP International Workshop on Robotic Perception*, 2008, pp. 23–32.

[11] G. Stillfried, U. Hillenbrand, M. Settles, and P. van der Smagt, "MRI-based skeletal hand movement model," in *The human hand - a source of inspiration for robotic hands*, R. Balaraman and V. Santos, Eds. Springer Tracts on Advanced Robotics, 2013, in print. Preprint available at http://elib.dlr.de/81117/.

[12] K. Meyberg and P. Vachenauer, *Höhere Mathematik 1*, ser. 4. Auflage. Berlin: Springer, 1999.

[13] J. A. Nelder and R. Mead, "A simplex method for function minimization," *The Computer Journal*, vol. 7, no. 4, pp. 308–313, 1965.

[14] Dexmart, "Deliverable D1.1 kinematic model of the human hand," The Dexmart Consortium, Tech. Rep., 2009. [Online]. Available: http://www.dexmart.eu/index.php?id=13735

[15] S. Mehrotra, "On the implementation of a primal-dual interior point method," *SIAM Journal on Optimization*, vol. 2, pp. 575–601, 1992.

[16] H. Choset, K. M. Lynch, S. Hutchinson, G. A. Kantor, W. Burgard, L. E. Kavraki, and S. Thrun, *Principles of Robot Motion: Theory, Algorithms, and Implementations*. Cambridge, MA: MIT Press, June 2005.

[17] J. Nocedal and S. J. Wright, *Numerical Optimization*, ser. Springer Series in Operations Research and Financial Engineering, T. V. Mikosch, S. I. Resnick, and S. M. Robinson, Eds. New York, NY, USA: Springer, 2006.

[18] A. R. Conn, N. I. M. Gould, and P. L. Toint, *Trust-region methods*. Philadelphia: SIAM, 2000.

[19] J. F. Soechting and M. Flanders, "Hand synergies during reach-to-grasp," *J Comput Neurosci*, vol. 4, pp. 29 – 46, 1997.

[20] S. Mulatto, A. Formaglio, M. Malvezzi, and D. Prattichizzo, "Animating a synergy-based deformable hand avatar for haptic grasping," in *International Conference EuroHaptics*, vol. 2, 2010, pp. 203–210.

[21] M. Bianchi, P. Salaris, and A. Bicchi, "Synergy-based hand pose sensing: Reconstruction enhancement (in press)," *International Journal of Robotics Research*, 2013.

[22] ——, "Synergy-based hand pose sensing: Optimal design (in press)," *International Journal of Robotics Research*, 2013.